SCIENCE CHINA Materials ARTICLES

mater.scichina.com link.springer.com

Published online 22 December 2017 | https://doi.org/10.1007/s40843-017-9161-4

Sci China Mater 2018, 61(3): 409–416

Spherical periodicity as structural homology of crystalline and amorphous states

Shuang Zhang[1], Dandan Dong[2], Zijian Wang[1], Chuang Dong[1*] and Peter Häussler[3]

ABSTRACT **It has been widely accepted that spherical periodicity generally dominates liquid and amorphous structure formation, where atoms tend to gather near spherically periodic shells according to Friedel oscillation. Here it is revealed that the same order is just hidden in the atomic global packing modes of the crystalline phases relevant to bulk metallic glasses. Among the multiple nearest-neighbor clusters developed from all the non-equivalent atomic sites in a given phase, there always exists a principal cluster, centered by which the spherical periodicity, both topologically and chemically, is the most distinct. Then the principal clusters plus specific glue atoms just constitute the cluster-plus-glue-atom structural units shared by both metallic glasses and the corresponding crystalline phases. It is further pointed out that the spherical periodicity order represents the common structural homology of crystalline and amorphous states in the medium-range through scrutinizing all binary bulk-glass-relevant phases in Cu-(Zr, Hf), Ni-(Nb, Ta), Al-Ca, and Pd-Si systems.**

Keywords: spherical periodicity order, Friedel oscillation, metallic glasses, cluster-plus-glue-atom model, principal cluster

INTRODUCTION

In the early stage of condensed matter formation, atoms tend to gather near specific shell positions following the so-called spherical periodicity order (SPO) [1], as determined by the charge screening effects according to Friedel oscillation [2]. Since amorphous structures are frozen states of the liquids, the same order is also recognized in metallic glasses according to a systematic analysis of the radial distribution functions (RDFs) of many thin-film metallic glasses [3]. The existence of SPO has also been confirmed in bulk metallic glass (BMG) structures, through both theoretical verifications [4,5] and simulated calculations [6,7]. The co-existence of SPO and crystal-like orders in BMGs provides a strong hint on the structural correlation between crystalline and amorphous states, and from the view of structural homology, SPO may also exist in crystalline phases relevant to BMGs. In particular, in accordance with the cluster-resonance model, developed by combining the cluster-plus-glue-atom model [8] with the global atom-electron wave resonance model (essentially SPO) [9], good metallic glass formers satisfy the universal cluster formula [cluster](glue atom)$_{1\text{ or }3}$ with 24 valence electrons, where the cluster is a nearest-neighbor coordination polyhedron and the one or three glue atoms are situated between the clusters. Such a structural description extends the previous models based primarily on local cluster configurations [10–12] to a longer-range model covering the cluster packing mode following SPO.

In constructing the cluster-plus-glue-atom model for metallic glasses, the clusters are directly derived from relevant devitrification crystalline phases, and it has been demonstrated that only the principal cluster [13], i.e., the most strongly bonded part in a given crystalline structure [14], enters into the relevant glass composition formula, signifying a close structural homology in terms of certain nearest-neighbor clusters shared by the crystalline and amorphous states. A well-verified example is the interpretation of $Cu_{64}Zr_{36}$ binary BMG using the cluster formula [Cu-Cu_7Zr_5]Cu, where [Cu-Cu_7Zr_5] is the principal cluster in the devitrification phase Cu_8Zr_3 and the total valence electron number per unit formula is quite close to 24, thus demonstrating a practical metallic glass composition design approach using the principal cluster [15]. It should be pointed out that in the cell structure of Cu_8Zr_3, there are eight non-equivalent atomic sites, centered by

[1] Key Laboratory for Materials Modification by Laser, Ion and Electron Beams (Dalian University of Technology (DUT)), Ministry of Education, Dalian 116024, China
[2] College of Physical Science and Technology, Dalian University, Dalian 116622, China
[3] Physics Institute, Chemnitz University of Technology, Chemnitz 09107, Germany
[*] Corresponding author (email: dong@dlut.edu.cn)

each developing a nearest-neighbor cluster. The principal one, [Cu-Cu_7Zr_5], is singled out for its largest cluster separation (i.e., minimum cluster overlap) and fairly dense packing among the eight clusters. This principal cluster, plus appropriate number of glue atoms, would generate the cluster formula unit for the corresponding metallic glass.

It is noticed that our previous investigations only unveiled the structural homology at the local cluster level in real space (***r***-space) [15]. The present paper will focus on the possible existence of SPO in the crystalline phases relevant to BMG formation and reveal the physical mechanism about the structural stability in reciprocal space (***k***-space). It will be shown that SPO is indeed hidden in the radial distribution of total atomic density, so long as centered by the principal clusters, thus demonstrating a nontrivial structural homology in short- to medium-range of crystalline and amorphous states covering both the local principal cluster level and the longer-range SPO. In the following, previous knowledge about SPO in metallic glasses will be briefly summarized. Then the analyses on the radial distribution of total atomic density will be conducted in the typical crystalline phases in binary BMG-forming systems such as Cu-(Zr, Hf), Ni-(Nb, Ta), Al-Ca and Pb-Si. Finally, the construction principle of the structural unit, i.e., a principal cluster with one or three glue atoms, will be pointed out, which reflects basically the first charge-neutral local unit in Friedel oscillation.

SPHERICAL PERIODICITY ORDER IN METALLIC GLASSES

SPO is triggered by minimizing the total energy along a self-organizing spherical resonance between the electronic system and the static atomic structure. In physics, SPO stems from Friedel oscillation [2], which is caused by the screening of electron cloud against localized perturbations [16,17]. In systems with long mean free paths of electrons, the effective Friedel oscillation potential of a charge at distance $\boldsymbol{r}$ is proportional to a damped cosine function, $\cos(2\boldsymbol{k}_F\cdot\boldsymbol{r}+\theta)/\hat{r}^3$ [1], with $\boldsymbol{k}_F$ as the Fermi vector and θ as the phase shift angle depending on the distances [18]. It is worth mentioning that for liquid and amorphous metals, at short- and medium-range distances, the effective pair potential is proportional to $-\sin(2\boldsymbol{k}_F\cdot\boldsymbol{r})/\hat{r}^3$ after a phase shift of $\theta=\pi/2$, as observed experimentally [9] and proved theoretically [19].

In the sine function, the zero points are located at $n\lambda_{Fr}$ and $(n+0.5)\lambda_{Fr}$, where n is a positive integer and the length unit is Friedel wavelength $\lambda_{Fr}=2\pi/(2k_F)$. The midpoints within the negative potential zones are then expressed as $\boldsymbol{r}_n=(n+1/4)\lambda_{Fr}$ [9], which defines the so-called SPO with a constant inter-shell spacing, λ_{Fr}. The negative potential zones are defined by their mid-points $\boldsymbol{r}_n$, and the positive potential zones by $\boldsymbol{r}_{n+0.5}$. In order to minimize the total energy of the whole system, atoms tend to gather in the favorable negative potential SPO-zones, $\boldsymbol{r}_n$. This is the so-called topological SPO. Thus, the first nearest-neighbor shell, where the atomic density is maximized, is situated within the $r_1=1.25\lambda_{Fr}$ zone. The chemical analogue refers to the preferential elemental occupancy in a spherically periodic manner satisfying atomic interactions, which further stabilizes the topological SPO. The atoms with electronegativities different from the central ones would prefer the negative potential SPO-zones, $\boldsymbol{r}_n$.

SPHERICAL PERIODICITY ORDER IN RADIAL DISTRIBUTION OF TOTAL ATOMIC DENSITY IN Cu_8Zr_3 PHASE

RDF is widely used to characterize the metallic glass structures [20]. For a random atom as the origin, RDF describes the probability of finding a neighboring atom at a distance between $\boldsymbol{r}$ and $(\boldsymbol{r}+\mathrm{d}\boldsymbol{r})$. The wavelength of RDF is equal to $2\pi/K_{pe}$ for an amorphous structure stabilized by Fermi sphere-Brillouin zone interaction. Here K_{pe} represents the diameter of the pseudo Brillouin or Jones zone. When the Friedel oscillation wave is in resonance with the static atomic wave, i.e., $2\pi/(2k_F)=2\pi/K_{pe}$, or $K_{pe}=2k_F$, the whole system reaches a stable state. In other words, this is the condition of the Brillouin or Jones zone in tangent with the Fermi surface. The resonance mechanism leads to the commensurate matching of the atomic RDF and the electronic Friedel oscillation potential function.

For a crystalline structure, the radial distribution of total atomic density, written as $\rho_t(\boldsymbol{r})=N/(4/3\pi\boldsymbol{r}^3)$, better reflects the radial atomic density perturbations with adding each spherical shell of atoms. Here, N refers to the total number of atoms (including the central one) enclosed within a specific spherical volume with radius $\boldsymbol{r}$. In fact, $\rho_t(\boldsymbol{r})$ reflects the charge shielding behavior in crystalline systems. If the interactions between charges are strong, the shielding would cause sharp oscillations. This radial distribution of total atomic density is actually a reinterpretation of RDF. It is then expected that SPO, if exists, can be read directly from such radial distribution of total atomic density $\rho_t(\boldsymbol{r})$.

The key to define SPO is to obtain Friedel wavelength λ_{Fr}, which is equal to $2\pi/(2k_F)$, or $2\pi/K_{pe}$. For a specific crystalline phase, the value of K_{pe} can be assessed directly from the most pronounced peak position in ***k***-space ex-

Table 1 Binary BMGs and their interpretations using cluster formulas derived from devitrification phases. Friedel wavelengths λ_{Fr} in crystalline phases are calculated *via* $\lambda_{Fr} = 2\pi/(2k_F)$, where the values of $2k_F$ are equal to the most intense peak positions K_{pe} according to the reported diffraction patterns. The last column illustrates the ratios between the measured cluster radii (approximately equal to the mean values of the innermost and outermost distances within the SPO r_1 zones) and the calculated Friedel wavelengths λ_{Fr}, which fall close to 1.25

Glass-forming compositions	Cluster formulas of relevant BMGs	Devitrification phases (structural types)	Cluster formulas of devitrification phases	Diameters of the Jones zones K_{pe} (nm^{-1})	Powder diffraction files	Friedel wavelengths for crystalline phases λ_{Fr} (nm)	Cluster radii (nm)	Cluster radii (λ_{Fr})
$Cu_{64}Zr_{36}$	$[Cu^4\text{-}Cu_7Zr_5]Cu$	$Cu_8Zr_3(Cu_8Hf_3)$	$[Cu\text{-}Cu_7Zr_3]$	27.515	42-1186	0.2284	0.2687	1.18
$Cu_{56}Zr_{44}$	$[Zr^2\text{-}Cu_{10}Zr_6]Zr$	$Cu_{10}Zr_7(Ni_{10}Zr_7)$	$[Zr\text{-}Cu_{10}Zr_4]Zr_2$	27.479	42-1187	0.2287	0.2954	1.29
$Cu_{50}Zr_{50}$	$[Zr\text{-}Cu_8Zr_6]CuZr_2$	CuZr(CsCl)	[Zr-Cu]	27.522	35-1092	0.2283	0.3044	1.33
$Cu_{65}Hf_{35}$	$[Cu^4\text{-}Cu_7Hf_5]Cu$	$Cu_8Hf_5(Cu_8Hf_5)$	$[Cu\text{-}Cu_7Hf_3]$	27.684	30-0477	0.2270	0.2669	1.18
$Nb_{38}Ni_{62}$	$[Ni^1\text{-}Nb_4Ni_8]Nb_2Ni$	$NbNi_3(Cu_3Ti)$	$[Ni\text{-}NbNi_2]$	31.854	65-0589	0.1972	0.2606	1.32
$Ni_{59.62}Ta_{41.38}$	$[(Ni,Ta)\text{-}Ni_6Ta_6]Ni_3$	$NiTa(Fe_7W_6)$	$[(Ni,Ta)\text{-}Ni_6Ta_2]Ta_4$	29.224	15-0270	0.2150	0.2683	1.25
$Al_{33.6}Ca_{66.4}$	$[Ca^5\text{-}Al_6Ca_8]Ca_3$	$Al_{14}Ca_{13}(Al_{14}Ca_{13})$	$[Ca\text{-}Al_6Ca_8]Al_8Ca_4$	22.188	Ref. [24]	0.2832	0.3583	1.27
$Pd_{82}Si_{18}$	$[Si\text{-}Pd_9]Si$	Pd_3Si (CFe_3)	$[Si\text{-}Pd_3]$	27.655	36-0932	0.2272	0.2694	1.19

perimentally. The thus-obtained values of λ_{Fr} are listed in Table 1. Then the radial distances $\boldsymbol{r}$ are normalized by λ_{Fr} as in the following figures. Since the electrons on the Fermi surface contribute biggest to the structural stability, the Friedel oscillation wave determined by $2k_F$ should be the most intense one among all the electron waves and dominates the whole system. The definition of λ_{Fr}, and hence the SPO-zones, in this way, satisfies the physical nature hidden in the structures themselves.

For example, Cu_8Zr_3 phase has the Cu_8Hf_3 structural type. According to the reported diffraction pattern, the diameter of the Brillouin or Jones zone, K_{pe}, i.e., $2k_F$, is 27.515 nm^{-1}, then the Friedel wavelength λ_{Fr} is approximate to 0.2284 nm, calculated with $\lambda_{Fr} = 2\pi/(2k_F)$. After normalizing radial distances $\boldsymbol{r}$ with λ_{Fr}, pronounced SPO clearly shows up in the density distribution profile centered by the principal cluster $[Cu^4\text{-}Cu_7Zr_5]$ (the superscript denotes the site sequence of the same atomic species), as shown in Fig. 1b, where the first three density maxima well fall within the first three negative potential zones r_1, r_2 and r_3.

Furthermore, chemical SPO is also noticed: the atoms showing strong interactions with the central ones tend to occupy the negative potential zones. As shown in Fig. 1b, Zr, showing strong negative enthalpy of mixing with the central Cu, is distributed only in the r_1 and r_2 zones, absent completely in the $r_{1.5}$ zone, though mixed occupancy occurs beyond the r_2 zone. In addition, the atomic concentrations contained in the Zr-shells are well above the average within the r_1 and r_2 zones as shown in Fig. 1b.

In the above example, only the profiles centered by the principal cluster $[Cu^4\text{-}Cu_7Zr_5]$ in Cu_8Zr_3 phase are analyzed. There are actually eight non-equivalent atomic sites in its unit cell. This $[Cu^4\text{-}Cu_7Zr_5]$ cluster possesses the highest cluster isolation, as measured by the longest distance between neighboring Cu^4 atoms, and a fairly high atomic dense packing efficiency [15]. As shown in Fig. 1c, the adjacent cluster $[Cu^4\text{-}Cu_7Zr_5]$ appears in the r_2 zone and shares some atoms with the central one, resulting in a reduced cluster formula $[Cu\text{-}Cu_7Zr_3]$ for the crystalline phase Cu_8Zr_3 (Table 1). On the other hand, in the corresponding BMG $Cu_{64}Zr_{36}$, the principal cluster $[Cu^4\text{-}Cu_7Zr_5]$ still dominates but is completely isolated to avoid any cluster-type local order from being extended to the longer-range. Therefore, this BMG is formulated as $[Cu\text{-}Cu_7Zr_5]Cu$.

In Fig. 2, all the eight radial distribution profiles of total atomic density in Cu_8Zr_3 phase are shown, and each has been scaled with the same wavelength λ_{Fr} calculated from the most intense peak position in the $\boldsymbol{k}$-space. The profile

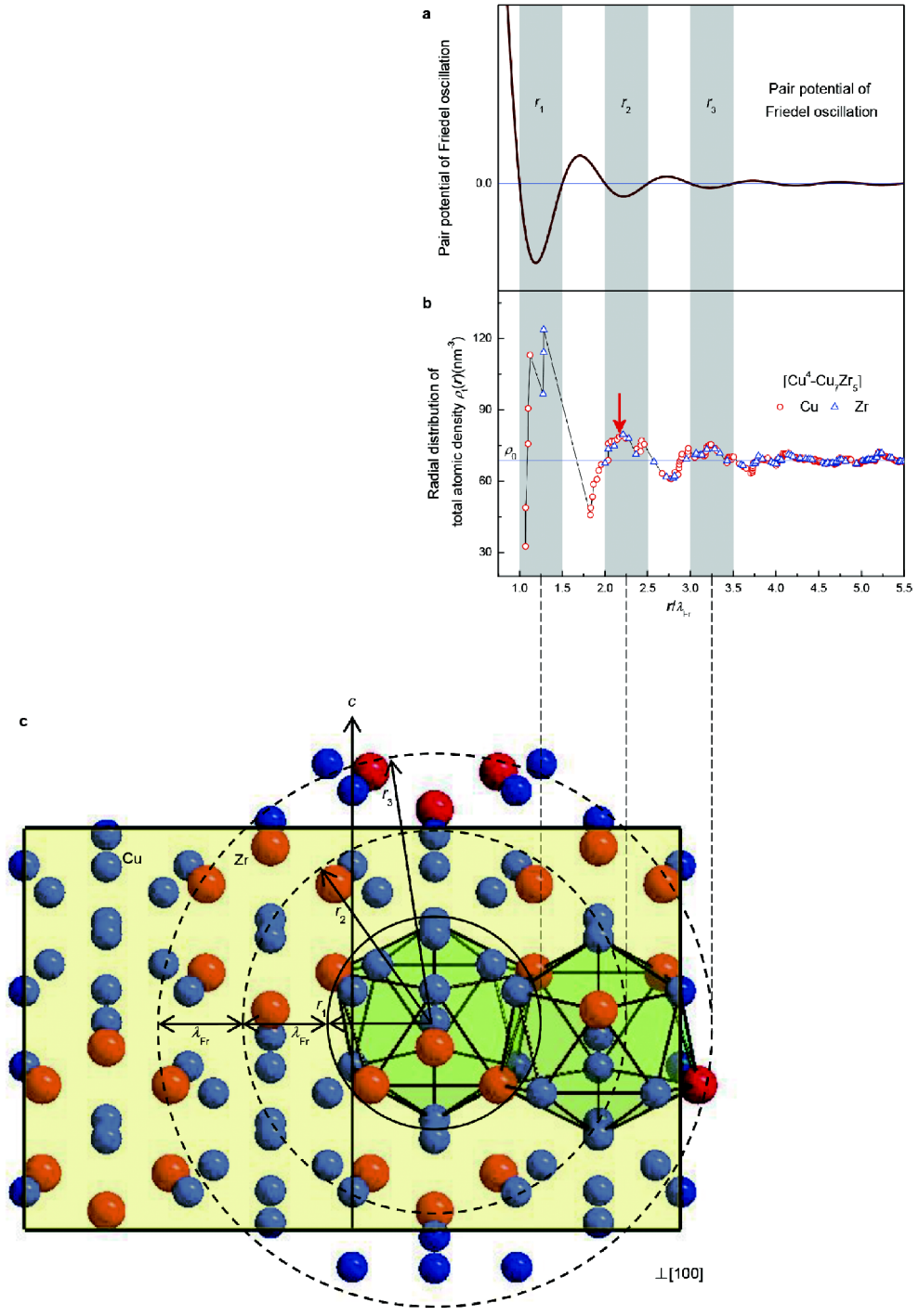

Figure 1 Correspondence between Friedel oscillation potential profile (a), atomic density distribution profile (b), and shelled structure (c). The latter two are both centered by the Cu^4 site of the Cu_8Zr_3 phase. The radial distribution profile is conducted on total atomic density $\rho_t(\boldsymbol{r}) = N/(4/3\pi\boldsymbol{r}^3)$ in Cu_8Zr_3 phase. N refers to the total number of atoms (including the central one) enclosed within a spherical radius $\boldsymbol{r}$. The horizontal line represents the mean particle density ρ_0. The downward arrow points to the first nearest-neighbor Cu^4 atoms, marking the distance between two neighboring [Cu^4-Cu_7Zr_5] clusters in the phase structure. The SPO-zones are shaded and marked by their respective $\boldsymbol{r}_n$. The abscissa is in the unit of Friedel wavelength $\lambda_{Fr} \approx 0.2284$ nm. Large and small spheres represent Zr and Cu atoms, respectively; and the two unit cells are shaded in (c).

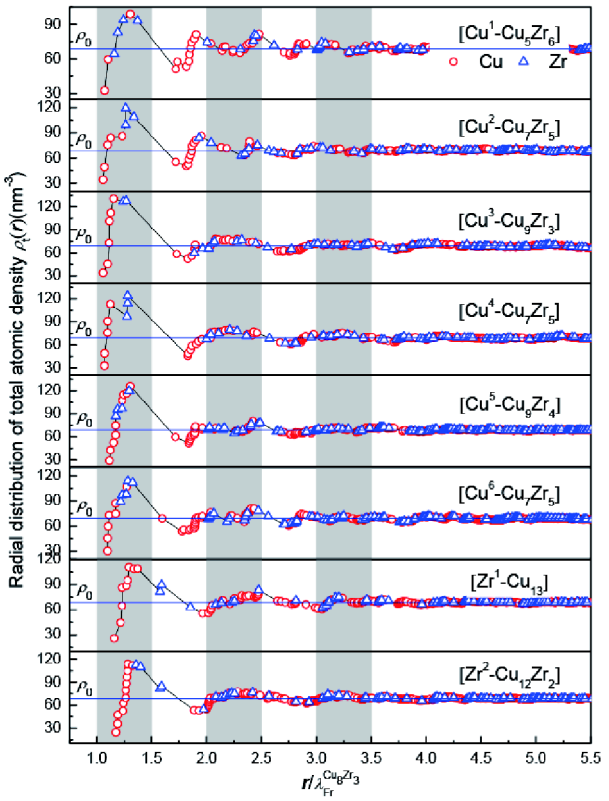

Figure 2 Radial distribution profiles of total atomic density centered by the eight clusters in Cu_8Zr_3 phase. The radial distances $\boldsymbol{r}$ are scaled with the Friedel wavelength $\lambda_{Fr} = 2\pi/(2k_F)$, with $2k_F$ obtained from the most intense peak position in its diffraction pattern using the resonance condition $2k_F = K_{pe}$.

centered by the principal cluster [Cu^4-Cu$_7$Zr$_5$] exhibits the most pronounced SPO. It is particularly noticed that the profile centered by Cu^3([Cu^3-Cu$_9$Zr$_3$] cluster) also shows apparently distinct SPO; however, the existence of Zr atoms in the $r_{1.5}$ zone signifies a weaker chemical SPO. The prominent SPO exhibited by the Cu^4-centered profile justifies the central role played by the principal cluster [Cu^4-Cu$_7$Zr$_5$] in stabilizing the overall structure, by matching the electron waves on the Fermi surface to the $\boldsymbol{r}$-space shells, characterized by $\lambda_{Fr} = 2\pi/(2k_F)$. In Fig. 2, it is noted that there are usually multiple high-density peaks within each $\boldsymbol{r}_n$ SPO-zone; however, high-density peaks always occur in $\boldsymbol{r}_n$ zones with negative potential, rather than in $\boldsymbol{r}_{n+0.5}$ zones with positive potential, which is characteristic of SPO. Such a principal-cluster-type local structure as well as the relevant SPO is then inherited between the crystalline devitrification phase and the amorphous/liquid counterpart, suggesting the common structural homology of the ordered crystalline states and the disordered precursors.

SPHERICAL PERIODICITY ORDER IN TYPICAL BINARY BULK-GLASS-FORMING CRYSTALLINE PHASES

Bulk-glass-forming compositions can be interpreted by the cluster-plus-glue-atom model according to the newly-refined composition design procedures for BMGs [21]. The key step is to determine the principal clusters in devitrification phases. Principal clusters, as the representative local structures [13,14], are commonly shared by both crystalline and amorphous states. All the presently known binary BMGs have been well interpreted *via* the cluster formula approach [15,22,23], as listed in Table 1. It is seen that each BMG has a crystalline counterpart, from which the principal cluster is obtained and the relevant cluster formula is constructed. The values of K_{pe} in the corresponding devitrification crystalline phases are obtained from their respective most intense peak positions in diffraction patterns (for $Al_{14}Ca_{13}$ phase, it is derived from Ref. [24]). It is worth mentioning that, for NiTa phase, the value of K_{pe} is 29.224 nm^{-1}, equal to the first pronounced peak position in $\boldsymbol{k}$-space, instead of another more intense one located at k = 51.083 nm^{-1} (which is much larger than the diameter of the first Brillouin or Jones zone). The measured cluster radii (approximately equal to the mean values of the innermost and outermost distances within the SPO r_1 zones) and the calculated Friedel wavelengths λ_{Fr} agree closely with the ideal relationship, i.e., cluster radius/λ_{Fr} = 1.25.

Strikingly similar SPO is present in all the radial distribution profiles of total atomic density centered by the principal clusters in the devitrification phases, as shown in Fig. 3. It is worth mentioning here that the SPO features hidden in the devitrification phases are reflected by the major density peaks, especially the first two peaks, falling closely within the corresponding negative potential zones $\boldsymbol{r}_n$ centered by $(n + 1/4)\lambda_{Fr}$, the ideal SPO positions in Friedel oscillation. In crystals, due to the anisotropy and periodicity constraints, SPO is not as evident as in the disordered amorphous states. The density peaks in the r_3 zones are relatively weak but are still recognizable in Cu_8Zr_3, CuZr, Cu_8Hf_3, NiTa, and $Al_{14}Ca_{13}$ phases. Specifically, in the profiles centered by the principal clusters [Cu^4-Cu$_7$Zr$_5$] [5], [Zr^2-Cu$_{10}$Zr$_6$] [5] (the two Zr^5 located near the $1.5\lambda_{Fr}$ boundary being attributed to the theoretical error), [Zr-Cu$_8$Zr$_6$] [15], and [Cu^4-Cu$_7$Hf$_5$] [5], the first three peaks are well located in the favorable negative potential zones r_1, r_2 and r_3, confirming the existence of topological SPO, though the peak in the r_3 zone in $Cu_{10}Zr_7$ phase is not so obvious. In addition, the atoms with

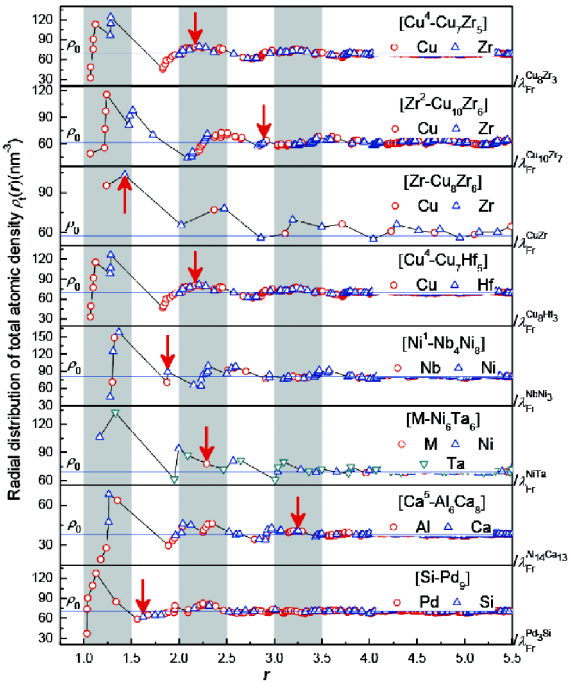

Figure 3 Radial distribution profiles of total atomic density centered by the principal clusters in typical devitrification phases relevant to binary BMGs, top-down: [Cu^4-Cu$_7$Zr$_5$] in Cu$_8$Zr$_3$, [Zr^2-Cu$_{10}$Zr$_6$] in Cu$_{10}$Zr$_7$, [Zr-Cu$_8$Zr$_6$] in CuZr, [Cu^4-Cu$_7$Hf$_5$] in Cu$_8$Hf$_3$, [Ni^1-Nb$_4$Ni$_8$] in NbNi$_3$, [M-Ni$_6$Ta$_6$] (M is a random mixture of Ni and Ta) in NiTa, [Ca^5-Al$_6$Ca$_8$] in Al$_{14}$Ca$_{13}$, and [Si-Pd$_9$] in Pd$_3$Si. The positions of adjacent identical clusters are arrowed.

electronegativities different from the central ones disappear completely in the positive potential $r_{1.5}$ zones, suggesting the chemical SPO. The SPO features in the profiles centered by the principal clusters [Ni^1-Nb$_4$Ni$_8$] [23], [M-Ni$_6$Ta$_6$] [5] (M is a random mixture of Ni and Ta), [Ca^5-Al$_6$Ca$_8$] [5] and [Si-Pd$_9$] [15] are relatively weak in comparison with those in the above-mentioned ones. Nevertheless, the atomic densities are always higher than the averages in the favorable negative potential zones, at least up to the r_2 zones (in the cases of [Ni^1-Nb$_4$Ni$_8$] and [Si-Pd$_9$], just to the r_2 zones). Mixed occupancy of both atomic species in the $r_{1.5}$ zones has weakened the chemical SPO in [Ni^1-Nb$_4$Ni$_8$], [Ca^5-Al$_6$Ca$_8$] and [Si-Pd$_9$]. For the principal cluster [M-Ni$_6$Ta$_6$], the chemical SPO is more pronounced when M is completely occupied by Ta than by Ni.

CLUSTER-PLUS-GLUE-ATOM STRUCTURAL UNITS OUT OF FRIEDEL OSCILLATION

From the radial distribution profiles of total atomic density, it is easily found that the most representative structural parts (principal clusters) are just located in the first negative Friedel oscillation potential zones where the central charge perturbations are the most intensely screened, with some neighboring atoms located in the first positive potential zones balancing the electronegativities of the local units. This is actually the cluster-plus-glue-atom model that has been used by us to interpret precisely many good BMGs and even some industrial alloys [25,26]. In the structural unit, the first nearest-neighbor cluster is located within the r_1 zone with the strongest negative potential, and the glue atoms preferentially fall within the $r_{1.5}$ zone with the strongest positive potential. We have shown, by analyzing existing and our own experiments, that the number of glue atoms is either 1 or 3 for all metallic glasses with the maximum glass forming abilities [8]. In addition, the formulas satisfy the 24-electron rule, i.e., the total number of valence electrons per unit cluster formula is close to 24, irrelevant to alloy systems and compositions [4,5]. Detailed procedures towards composition design for metallic glasses of high glass forming abilities have been provided [15,21]. Since SPO is also prominent in the corresponding devitrification phases, the short-range-order heritage in terms of cluster-plus-glue-atom model evidently exists in the amorphous and the corresponding crystalline states, thus rationalizing the use of the cluster formula approach as BMG interpretation and eventually a design tool.

For ideal amorphous structures, there is no sharing between the cluster-based structural units; the atomic radial distribution would conform to SPO perfectly up to the medium-range. While for crystalline structures, due to the existence of anisotropic restrictions and periodic potential barriers, the structural units usually overlap with neighboring ones, leading to the weakened SPO as already mentioned. As arrowed in Fig. 3, the adjacent structural units fall within the r_3 zone in Al$_{14}$Ca$_{13}$ phase, while those in other phases are all located at the distances shorter than r_3: the neighboring structural units in Cu$_{10}$Zr$_7$ phase fall within the $r_{2.5}$ zone; those in Cu$_8$Zr$_3$, Cu$_8$Hf$_3$ and NiTa phases within the r_2 zones; those in NbNi$_3$ and Pd$_3$Si phases in the $r_{1.5}$ zones; and those in CuZr phase in the r_1 zone.

CONCLUSIONS

After analyzing the radial distribution of total atomic density in devitrification phases relevant to binary BMGs in systems Cu-(Hf, Zr), Ni-(Nb, Ta), Al-Ca and Pd-Si, spherical periodicity order is unveiled in all of the devitrification phases, so long as centered by the principal clusters. The principal clusters plus specific glue atoms

then construct the structural units shared by the crystalline and amorphous states. These results suggest the nontrivial structural homology between metallic glasses and the corresponding crystalline phases both at the local unit level (covering the principal cluster plus glue atoms) and in the medium-range *via* spherical periodicity order.

Received 20 July 2017; accepted 17 November 2017; published online 22 December 2017

1 Häussler P. Interrelations between atomic and electronic structures—liquid and amorphous metals as model systems. Phys Rep, 1992, 222: 65–143
2 Friedel J. Electronic structure of primary solid solutions in metals. Adv Phys, 1954, 3: 446–507
3 Häussler P, Barzola-Quiquia J. Spherical periodicity, an intermediate step to long-range order. J Non-Crystalline Solids, 2002, 312-314: 498–501
4 Han G, Qiang J, Li F, *et al.* The e/a values of ideal metallic glasses in relation to cluster formulae. Acta Mater, 2011, 59: 5917–5923
5 Luo L, Chen H, Wang Y, *et al.* 24 electron cluster formulas as the 'molecular' units of ideal metallic glasses. Philos Mag, 2014, 94: 2520–2540
6 Liu X, Xu Y, Hui X, *et al.* Metallic liquids and glasses: atomic order and global packing. Phys Rev Lett, 2010, 105: 155501
7 Wu Z, Li M, Wang W, *et al.* Hidden topological order and its correlation with glass-forming ability in metallic glasses. Nat Commun, 2015, 6: 6035
8 Dong C, Wang Q, Qiang J, *et al.* From clusters to phase diagrams: composition rules of quasicrystals and bulk metallic glasses. J Phys D-Appl Phys, 2007, 40: R273–R291
9 Häussler P. A new hume-rothery phase with an amorphous structure in noble-metal/simple-metal alloys. J Phys Colloques, 1985, 46: C8-361–C8-365
10 Bernal J. Geometry of the structure of monatomic liquids. Nature, 1960, 185: 68–70
11 Gaskell P. A new structural model for transition metal–metalloid glasses. Nature, 1978, 276: 484–485
12 Miracle D. The efficient cluster packing model–an atomic structural model for metallic glasses. Acta Mater, 2006, 54: 4317–4336
13 Chen J, Wang Q, Wang Y, *et al.* Cluster formulae for alloy phases. Philos Mag Lett, 2010, 90: 683–688
14 Du J, Wen B, Melnik R, *et al.* Determining characteristic principal clusters in the "cluster-plus-glue-atom" model. Acta Mater, 2014, 75: 113–121
15 Dong D, Zhang S, Wang Z, *et al.* Composition interpretation of binary bulk metallic glasses *via* principal cluster definition. Mater Des, 2016, 96: 115–121
16 Harrison WA. Solid State Theory. New York: McGraw-Hill, Inc., 1970
17 Ziman JM. Principles of the Theory of Solids. Cambridge: Cambridge university press, 1972
18 Hafner J, Heine V. The crystal structures of the elements: pseudopotential theory revisited. J Phys F-Met Phys, 1983, 13: 2479–2501
19 Kroha J, Huck A, Kopp T. Coulomb interaction and disorder at $q=2k_F$: a novel instability of the Fermi sea and implications for amorphous alloys. Phys Rev Lett, 1995, 75: 4278–4281
20 Zallen R. The Physics of Amorphous Solids. New York: John Wiley & Sons, Inc., 1983
21 Wang Z, Qiang J, Wang Y, *et al.* Composition design procedures of Ti-based bulk metallic glasses using the cluster-plus-glue-atom model. Acta Mater, 2016, 111: 366–376
22 Wang Z, Dong D, Zhang S, *et al.* Characteristics of cluster formulas for binary bulk metallic glasses. J Alloys Compd, 2016, 654: 340–343
23 Zhang S, Dong D, Wang Z, *et al.* Composition formulas of Ni-(Nb, Ta) bulk metallic glasses. Intermetallics, 2017, 85: 176–179
24 Huang B, Corbett J. Two new binary calcium−aluminum compounds: $Ca_{13}Al_{14}$, with a novel two-dimensional aluminum network, and Ca_8Al_3, an Fe_3Al-type analogue. Inorg Chem, 1998, 37: 5827–5833
25 Hong H, Wang Q, Dong C, *et al.* Understanding the Cu-Zn brass alloys using a short-range-order cluster model: significance of specific compositions of industrial alloys. Sci Rep, 2014, 4: 7065
26 Hong H, Wang Q, Dong C. Composition formulas of Cu-Ni industrial alloy specifications. Sci China Mater, 2015, 58: 355–362

Acknowledgements This work was supported by the Science Challenge Program (JCKY2016212A504) and the National Natural Science Foundation of China (11674045).

Author contributions Zhang S conducted the calculations, analyzed the data, and wrote the paper. Dong D and Wang Z participated in the discussions about the cluster models. Dong C proposed the cluster model theory and revised the manuscript. Häussler P helped with introducing Friedel oscillation and spherical periodicity order into the cluster model.

Conflict of interest The authors declare that they have no conflict of interest.

Shuang Zhang is a PhD candidate majored in condensed matter physics at the School of Materials Science and Engineering in DUT. Her research interests include structural modeling of metallic glasses and solid solutions, composition design of alloys, structural origin of simple crystals, and structural homology between ordered and the corresponding disordered states.

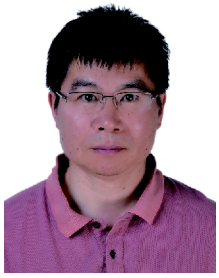

Chuang Dong is a professor at the Key Laboratory of Materials Modification, DUT. He obtained his PhD degree in materials science in 1991 at INPL, France. He owned the titles of the Outstanding Young Researcher in 1995 and Changjiang Professor in 2005, respectively. His research interests include structural modeling of disordered materials, alloy design, and surface modification.

晶态与非晶态结构的球周期同源性

张爽[1], 董丹丹[2], 王子鉴[1], 董闯[1*], Peter Häussler[3]

摘要 球周期在液体与非晶的结构形成过程中占有主要地位, 根据Friedel振荡理论, 原子倾向于聚集在球周期壳层上. 本文提出在非晶晶体相结构中依然隐藏着球周期序列. 在一个给定的相中, 所有非等效原子占位皆衍生出相应的最近邻团簇, 其中必然存在一个具有代表性的主团簇, 以其为中心时, 球周期最明显. 该主团簇加上特定的连接原子组成了对应非晶态的团簇加连接原子结构单元. 本文通过全面分析Cu-(Zr, Hf), Ni-(Nb, Ta), Al-Ca与Pd-Si二元块体非晶形成体系中的晶化相, 进一步指出球周期序代表了晶态与非晶态在中程序的结构同源性.

